Restricted electron motion in a one-dimensional organic conductor: Pulsed-gradient spin-echo ESR in (fluoroanthene)$_2$PF$_6$

N. Kaplan
Racah Institute, Hebrew University, Jerusalem, Israel

E. Dormann and R. Ruf
Physikalisches Institut, Universität Karlsruhe, D-76128 Karlsruhe, Germany

A. Coy and P. T. Callaghan
Department of Physics, Massey University, Palmerston North, New Zealand

(Received 10 February 1995)

The pulsed-gradient spin-echo electron spin resonance method has been used to measure the restricted diffusion of electrons along fluoranthene channels in the quasi-one-dimensional organic conductor (fluoroanthene)$_2$PF$_6$. This type of experiment allows one to measure the echo attenuation both as a function of diffusional observation time Δ and effective scattering wave-vector amplitude q. In these experiments Δ was varied between 10 and 20 μs, while q values of up to 2.5×10^4 m^{-1} were employed, enabling dynamic spatial resolution on the micron scale. The echo attenuation data are broadly characteristic of one-dimensional electron diffusion within the confines of an ensemble of wells, in which the well dimension l is characterized by a distribution $p(l)=l\bar{l}^{-2}\exp(l/\bar{l})$. Subtle deviations in this behavior can be modeled both by allowing for relaxation effects at the well boundaries, or by allowing for weak boundary permeability.

I. INTRODUCTION

The one-dimensional (1D) organic metals form a class of materials in which the conduction-electron mobility is highly anisotropic with respect to the crystallographic axes. This anisotropy is manifested in conductivity and in electron self-diffusion measurements and, as a consequence, these materials are known as quasi-one-dimensional. The mechanisms which limit electron mobility along the conducting channels in such systems are of considerable theoretical interest, and it is clear that a deeper understanding of these effects will have practical significance.

The present paper concerns a pulsed-gradient spin-echo electron spin resonance (ESR) study of the diffusional motion of conduction electrons, along fluoranthene channels in the one-dimensional organic metal (fluoranthene)$_2$PF$_6$. Previous measurement of self-diffusion of (FA)$_2$PF$_6$ by ESR methods (Ref. 1) have indicated that the upper limit for diffusion perpendicular to the conducting channels is at three orders of magnitude smaller than in the longitudinal direction. In a recent study of this system using steady gradient spin-echo methods,[2] the time (τ) dependence of the echo amplitude was fitted using a model comprising both transverse (T_2) relaxation and diffusive relaxation effects. The echo attenuation for unrestricted diffusion in the presence of a steady gradient is due to Torrey,[3] and given by

$$E\sim\exp\left[-\frac{2\tau}{T_2}\right]\exp(-\tfrac{2}{3}D\gamma^2G^2\tau^3)\ . \tag{1}$$

The steady gradient data for (FA)$_2$PF$_6$ strongly deviated from the simple τ^3 dependence expected for free diffusion, but was able to be represented more closely by the restricted diffusion model of Neumann.[4] In particular, the echo attenuation was fitted using an expression based on the assumption of confinement in one-dimensional wells of length l in which the distribution of well sizes is given by the density distribution $P(l)=\bar{l}^{-1}\exp(-l/\bar{l})$ and the consequent weight function, which represents the electron contribution to the echo, is given by $p(l)=l\bar{l}^{-2}\exp(-l/\bar{l})$. The free parameters of the fit are therefore T_2, D, and $\bar{l}$, and yielded values of 6.7 μs, 1.8×10^{-4} m^2 s^{-1}, and 96 μm, respectively.

The steady gradient approach, while providing important insight, suffers from a number of defects. First, the Neumann expression is based on an assumption of Gaussian spin-phase distribution,[4] and gives only an approximate description of the echo attenuation. The method does not take account of transverse relaxation which depends upon well size, for example due to decoherence effects caused by electron scattering at the boundary. This particular problem is complicated by the need to separate diffusional and T_2 relaxation effects in the analysis of the echo time dependence.

An alternative approach to the problem is provided by the pulsed-gradient spin-echo (PGSE) (Ref. 5) ESR method in which the spin echo is attenuated due to spin motion over the time Δ between two sharply defined gradient pulses of duration δ and amplitude **g**. In this experiment the attenuation at a fixed time is examined as a function of gradient strength. Provided that the gradient pulses are sufficiently narrow, this experiment provides a

0163-1829/95/52(23)/16385(10)/$06.00

direct measurement of the average propagator of the spin motion via a Fourier relation akin to that which applies in inelastic neutron scattering.[6,7] Indeed, the method allows one to define an effective scattering wave vector $\mathbf{q}$, which is determined by the gradient pulse time integral $\mathbf{q}=(2\pi)^{-1}\gamma\int\mathbf{g}(t)dt$.

One particular advantage of the PGSE approach is that the propagator for the one-dimensional well, incorporating relaxation at the walls, is known exactly.[8] Furthermore, the method directly and independently probes both time and wave-vector domains, providing a test of internal consistency in the modeling process. The principal challenge faced by PGSE ESR concerns the use of short and intense gradient pulses, on the order of 1 μs in duration and 0.1 T m^{-1} in amplitude.

II. EXPERIMENT

The apparatus used to carry out PGSE ESR experiments on the microsecond time scale has been described in detail elsewhere.[9] The system employs three orthogonal gradient coils[10] of sensitivity 0.2 T m^{-1} A^{-1}. In order to generate gradient pulses of sufficiently short duration, we have utilized a home-built pulsed-current driver based on the clipped L-C resonance idea of Conradi *et al.*[11] This driver enables semisinusoidal current pulses of any duration δ down to 2 μs and at peak field gradients up to 1.0 T m^{-1}, to be easily realized with our coils using a small 50-V dc power supply. In the experiments reported here the saddle G_x coil, coaxial with the rf coil, was used for the pulsed gradients, while the remaining quadrupolar coils were used to shim the local magnetic field.

In order to minimize eddy currents associated with rapidly switched gradients, we have placed the probe head in the fringe field outside a 7.0-T NMR cryomagnet. The fringe field is highly stable and free from any component of field ripple that is usually present in electromagnets. The required static field of approximately 10.5 mT (for ESR at 300 MHz) was obtained by adjusting the position of the sample coil to a radial distance of $\sim$87 cm from the magnet axis, in the equatorial plane of the magnet coil assembly. The field at this position is vertical and antiparallel to the field in the center of the magnet, and the expected static radial gradient component of some 0.03 T m^{-1} could be easily shimmed out by small dc current in the three-axis gradient coil assembly.

PGSE ESR experiments were carried out at Massey University using a well-characterized single-crystal sample of $(FA)_2PF_6$ (Ref. 12) at room temperature. A Bruker AMX300 NMR spectrometer was used to generate a 300-MHz spin-echo sequence comprising a 90_x-τ-180_y-τ pulse train in which the 90_x and 180_y hard pulses had durations of 0.2 and 0.4 μs, respectively, thus providing an effective excitation bandwidth of 2.5 MHz. The long axis of the crystal sample, nominally in the direction of the conducting channels, was oriented manually along the direction of G_x with an estimated accuracy of $\pm 15°$. Data were acquired at 10 M samples s^{-1} with an acquisition bandwidth of 5 MHz. Receiver dead time allowed fully recovered echo signals only for $\tau \geq 4$ μs. Free induction decay (FID) signals from a single acquisition following a 90° rf pulse exhibited a T_2^* of around 6 μs, consistent with the earlier spin-echo results. The near absence of inhomogeneous broadening indicates the effectiveness of shimming and the absence of residual steady gradients.

In the PGSE sequence, weak static gradients were present, probably due to slowly decaying eddy currents caused by the effect of the rapidly switched field-gradient pulses in the vicinity of the rf shield. Figure 1 shows a typical example of an on-resonance spin-echo signal, obtained by signal averaging after 1000 excitations where the echo time 2τ is 16 μs. In all experiments reported here the δ pulses were positioned immediately after each of the rf pulses, thus implying $\Delta=\tau$. This helped minimize attenuation artifacts caused by residual eddy fields. Note that for semisinusoidal gradient pulses of amplitude g, the reciprocal space vector $\mathbf{q}$ has magnitude q given by $\pi^{-2}\gamma\delta g$, where δ is the time between the two zero crossings of the current.

III. PGSE THEORY

Here we shall summarize the theory of pulsed-gradient spin-echo (PGSE) ESR (Refs. 6, 18, and 13) as it applies to restricted diffusional motion of electrons located within an array of one-dimensional wells, and where the applied magnetic gradient direction is applied parallel to the diffusion axis. Two principal models will be considered. In the first the electrons are completely confined in the wells but may suffer some relaxation effects in collision with the barriers. In the second, some hopping between wells is permitted. A key assumption of the analysis is that the spins move an insignificant distance during the gradient pulse itself, or in other words, $\delta \ll l^2/D$ where l is the interbarrier spacing. However, it has been shown that even where significant motion does occur, the narrow pulse analysis may still be applied but with the effect that the apparent displacement of the spins is reduced, leading to an apparently smaller well size.[14]

Using the conditional probability $P_s(x|x',\Delta)$ that an

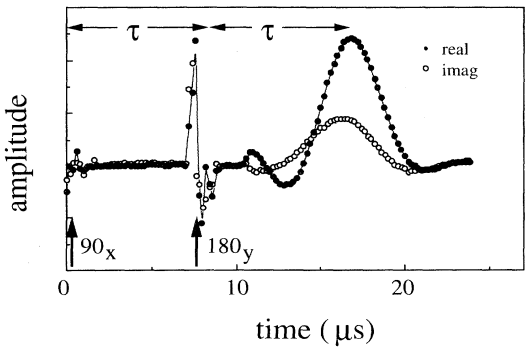

FIG. 1. Real and imaginary echo signals from a 90_x-τ-180_y spin-echo sequence ($\tau=7.8$ μs) after signal averaging from 1024 transients. The acquisition begins 0.5 μs before the first rf pulse, although the correct phase cycling for signal coaddition does not begin until 0.5 μs following the second pulse. The additional delay before the signal appears is due to the 4-μs dead time.

electron starting at position x on the well axis will move to position x' over the time Δ, we may write the echo attenuation as[5,6]

$$E(q,\Delta)=\int \rho(x)P_s(x|x',\Delta)\exp[i2\pi q(x'-x)]dx\,dx' , \tag{2}$$

where $\rho(x)$ is the starting spin density, the quantity mapped in conventional NMR or ESR imaging, and corresponds to the pore electron density function. $\int\rho(x)P_s(x|x',\Delta)dx$ defines the average propagator,[6,13] $\overline{P_s}(X,\Delta)$, the probability that an electron at any starting position is displaced by $X=x'-x$ over time Δ. Consequently Eq. (2) may be written[6]

$$E(q,\Delta)=\int \overline{P_s}(X,\Delta)\exp[i2\pi qX]dX . \tag{3}$$

Clearly inverse Fourier transformation of $E(q,\Delta)$ with respect to q returns an image of the average propagator $\overline{P_s}$. In this sense PGSE ESR is analogous to an imaging experiment, the difference here being that electron-spin motions rather than positions are mapped.

In free diffusion the propagator is Gaussian, and the echo dependence will also have a Gaussian dependence on q, namely,

$$E(q,\Delta)=\exp(-4\pi^2q^2D\Delta) , \tag{4}$$

i.e., the signal reverts to the well-known Stejskal-Tanner relation.[5]

A. Confinement within wells

We now consider the case[15] where the electrons are completely confined by impenetrable barriers to diffusion. For a one-dimensional well whose barriers are separated by a distance l, the electron diffusion will appear to be unrestricted for $\Delta \ll l^2/2D$, whereas for $\Delta \gg l^2/2D$ all electrons, irrespective of starting position, can be found anywhere within the pore, and the mean-squared displacement will appear to be time-independent and on the order of l^2. This long-time limit leads directly to a diffraction interpretation since, for $\Delta \gg l^2/2D$, $P_s(x|x',\Delta)$ reduces to $\rho(x')$, the pore molecular density function, while the averaged propagator $\overline{P_s}(X,\infty)$ becomes an autocorrelation function of $\rho(x')$,

$$\overline{P_s}(X,\infty)=\int \rho(x+X)\rho(x)dx . \tag{5}$$

In consequence the echo attenuation function reduces to the Fourier power spectrum of $\rho(\mathbf{r}')$,

$$E(q,\infty)=|S(q)|^2 . \tag{6}$$

For the one-dimensional well this is precisely the diffraction pattern of a single slit, namely,

$$|S(q)|^2=\frac{2[1-\cos(2\pi ql)]}{(2\pi ql)^2} . \tag{7}$$

It is important to note that Eq. (7) is not only independent of the observation time Δ but is also independent of the microscopic self-diffusion coefficient D. This marks an important distinction between PGSE ESR and the steady gradient spin-echo where D is a key parameter in the analysis of the echo attenuation process. In the long-time-scale limit of PGSE ESR the actual diffusion rate is important only in determining the onset of the Δ-independent regime. Remarkably, while the regime is labeled "long-time scale," it is very closely approximated even when $\Delta \sim l^2/2D$, a factor which enhances the usefulness of the model.

In the situation encountered here the electrons occupy a distribution of wells of different size l, so that an average structure factor can be obtained by integrating over the assumed distribution function, $p(l)=\bar{l}^{-2}\exp(-l/\bar{l})$. The result is clearly an approximation since the pore equilibration condition $\Delta \gtrsim l^2/2D$ must break down for the largest values of l. Provided, however, that $\bar{l}$ is not too large, this fraction of electrons will be small and the average structure factor will be useful. The result of integrating Eq. (7) over the distribution $p(l)$ is simply

$$\overline{|S_0(q)|^2}=(4\pi^2q^2\bar{l}^2)^{-1}\ln(1+4\pi^2q^2\bar{l}^2) . \tag{8}$$

Some further insight regarding the effect of the distribution of well sizes may be gained by pursuing the diffraction model under the influence of the small scattering wave-vector approximation, i.e., $2\pi qX \ll 1$. In this case the echo attenuation is given by[16] $\exp[-\frac{1}{2}(2\pi q)^2\overline{X^2}]$. For the case of the one-dimensional well in the long-time limit, one may obtain a direct model-independent measurement of the length distribution parameter $\bar{l}^2$ without needing the particular functional form of the distribution. To the extent that the long-time small q conditions are met effectively for all l values in the distribution, we may describe the amplitude of the echo signal, arising from the entire distribution ensemble, by the expression

$$E(q,\infty)=\exp[-(2\pi q)^2\tfrac{1}{12}\bar{l}^2] . \tag{9}$$

This simple diffraction picture for PGSE ESR of trapped electrons, and its further extension to low wave vector, is very helpful in providing theoretical insight. However, the need for many of the assumptions involved may be removed by a more exact theory, and this will be the approach adopted in Sec. III B.

B. Relaxation and finite observation time effects

In addition to the finite gradient pulse width effects referred to above, two other factors result in modifications to the simple diffraction theory. The first concerns the problem of the long-time-scale approximation. Given the wide distribution of l values expected in the fluoranthene samples, many conducting channels will exhibit well sizes for which $\Delta < l^2/2D$. The long-time-scale approximation may be avoided in a more sophisticated theory. The second issue concerns the need to allow for relaxation effects. Given the relatively short relaxation times that apply for the conduction electrons, it is necessary to work at spin-echo durations for which the attenuation due to normal (T_2) relaxation is substantial. This raises concerns about T_2 values which may depend on well dimension, thereby engendering unequal weighting to the ap-

parent spin populations and deviations in the apparent well sizes determined from the diffraction model.

Recently, an exact expression has been derived which accounts for both such effects.[8,17] The analysis is based on an eigenmode expansion in which the boundary condition for the spin density, $D\hat{\mathbf{n}}\cdot\nabla\rho+M\rho=0$, allows for both reflection and relaxation at the walls. Here D is the *microscopic* diffusion constant while M is the average magnetization sink density on the boundary surface with normal $\hat{\mathbf{n}}$. These determine the parameter set $\{\xi_n,\zeta_n\}$ given by the roots of

$$\xi_n\tan\xi_n=\frac{Ml}{2D} \quad \text{and} \quad \zeta_n\cot\zeta_n=-\frac{Ml}{2D} . \tag{10}$$

For the PGSE ESR pulse sequence used here, the average propagator and the echo attenuation are given, respectively, as[17]

$$\begin{aligned}\overline{P_s}(X,\Delta)=&\sum_{n=1}^{\infty}\exp\left[-\frac{(2\xi_n)^2D\Delta}{l^2}\right]l^{-2}[1+\sin(2\xi_n)/2\xi_n]^{-1}\\&\times([l-X+(l/4\xi_n)\{\sin(2\xi_n-4\xi_nX/l)+\sin(2\xi_n)\}]\cos(2\xi_nX/l)\\&+(l/4\xi_n)\{\cos(2\xi_n-4\xi_nX/l)-\cos(2\xi_n)\}\sin(2\xi_nX/l))\\&+\sum_{m=1}^{\infty}\exp\left[-\frac{(2\zeta_m)^2D\Delta}{l^2}\right]l^{-2}[1-\sin(2\zeta_m)/2\zeta_m]^{-1}\\&\times([l-X-(l/4\zeta_m)\{\sin(2\zeta_m-4\zeta_mXl)+\sin(2\zeta_m)\}]\cos(2\zeta_mXl)\\&-(l/4\zeta_m)\{\cos(2\zeta_m-4\zeta_mXl)-\cos(2\zeta_m)\}\sin(2\zeta_mXl)) ,\end{aligned} \tag{11}$$

$$\begin{aligned}E_l(q,\Delta)=&\sum_{n=1}^{\infty}\exp\left[-\frac{(2\xi_n)^2D\Delta}{l^2}\right]2[1+\sin(2\xi_n)/2\xi_n]^{-1}\frac{[(\pi ql)\sin(\pi ql)\cos\xi_n-\xi_n\cos(\pi ql)\sin\xi_n]^2}{[(\pi ql)^2-\xi_n^2]^2}\\&+\sum_{m=1}^{\infty}\exp\left[-\frac{(2\zeta_m)^2D\Delta}{l^2}\right]2[1-\sin(2\zeta_m)/2\zeta_m]^{-1}\frac{[(\pi ql)\cos(\pi ql)\sin\zeta_m-\zeta_m\sin(\pi ql)\cos\zeta_m]^2}{[(\pi ql)^2-\zeta_m^2]^2} .\end{aligned} \tag{12}$$

In the analysis of the results presented here, we shall use the exact expression for the echo attenuation given by Eq. (12), weighted by the well size distribution function, $p(l)$, i.e.,

$$E(q,\Delta)=\int_0^{\infty}p(l)E_l(q,\Delta)dl . \tag{13}$$

We refer to this depiction expressed in Eqs. (12) and (13) as the impenetrable relaxing wall (IRW) model. Two limiting cases for relaxation apply, depending on whether $Ml/2D$ is greater or less than unity. While these limits help explain the role of relaxation for the situation encountered in the PGSE ESR experiments on fluoranthene, it is unnecessary to make such assumptions in fitting the data. In both cases small wells suffer proportionately greater relaxation. The influence of relaxation is therefore to diminish the contribution to $E(q,\Delta)$ from the smaller wells, thus preferentially reducing the echo amplitude at large q.

C. Well hopping

The facility to move between wells suggests that, instead of being restricted to the dimensions of the local well, each electron, over a sufficiently long time scale, will experience a long-range mobility characterized by an effective diffusion coefficient D_{eff}. This provides a sharp contrast with the model leading to Eqs. (12) and (13), in which electrons suffer relaxation at the well boundaries but no hopping between wells is possible.

In allowing for migration of electrons between wells, two different cases are considered. In the first, the migration occurs due to displacements along the chain in which a small fraction of electrons pass the barrier to a neighboring well rather than being reflected back into the same well. For such a model well hopping clearly depends on the electrons making collisions with the well ends, and can therefore lead to rapidly enhanced migration only if the barriers are highly permeable. We refer to this as the permeable well (PW) model.

In the second model, transverse migration between chains allows electrons to move to a well of different l and center positions. This latter process does not in fact require boundary collisions but, instead, the rate of well hopping is determined by the transverse diffusion rate alone. Irrespective of local barrier permeability, if this chain hopping is sufficiently rapid to allow electrons to move freely between chains in which the position and spacings of barriers are randomly varying, then the effect is that net migration parallel to the chain directions will be rapid and the effective longitudinal diffusion coefficient will approach the local (free) diffusion value D. This transverse migration (TM) model differs strongly from the PW model in its predictions for the echo attenuation function.

The first (PW) model of well hopping has been treated in detail in an earlier paper.[7] Two assumptions are crucial. In the first, the so-called "pore equilibration" condi-

tion, we assume that permeability is weak and that the electrons will experience sufficient numbers of collisions that the diffraction effects of motion within the well may be separated from the interpore effects. For interwell spacings comparable with the well size, the equilibration condition is satisfied provided $\Delta \gtrsim l^2/2D$ and $D_{\text{eff}} \ll D$. In the second assumption, we presume that the probability of well hopping in a given time interval is independent of the distance to the first neighboring well. Under these conditions it may be shown that the echo attenuation is given by

$$E(q,\Delta)=\overline{|S_0(q)|^2}\exp[-\lambda D_{\text{eff}}\Delta(1-\mathsf{F}\{h(X)\}]\,, \tag{14}$$

where $h(X)$ represents the distribution of neighboring well-center displacements, and $\mathsf{F}\{\ \}$ is the Fourier transform operator. The variable λ is determined by the relationship

$$2D_{\text{eff}}\Delta=(2\pi)^{-2}\partial^2/\partial q^2\exp[-\lambda D_{\text{eff}}\Delta(1-\mathsf{F}\{h(X)\}]|_{q=0}\,. \tag{15}$$

While $\overline{|S_0(q)|^2}$ is given by Eq. (7), the function $h(X)$ is obtained by considering two neighboring wells of spacing l_1 and l_2, respectively. Because the well centers are separated by $X=(l_1+l_2)/2$, the probability distribution $h(X)$ is given by

$$\begin{aligned} h(X)&=2\int_0^{2X}p(l_1)p(2X-l_1)dl_1 \\ &=\tfrac{8}{3}X^3\bar{l}^{-4}\exp(-2X/\bar{l})\,. \end{aligned} \tag{16}$$

On Fourier transformation of $h(X)$ and evaluation of the constant, λ, we find

$$E(q,\Delta)=(4\pi^2q^2\bar{l}^2)^{-1}\ln(1+4\pi^2q^2\bar{l}^2)\exp\left[-\frac{2D_{\text{eff}}\Delta}{5\bar{l}^2}\left[1-\frac{1-6(\pi q\bar{l})^2-(\pi q\bar{l})^4}{[1+(\pi q\bar{l})^2]^4}\right]\right]\,. \tag{17}$$

It should be noted that the assumption of equal well hopping probability is not absolutely necessary. Indeed, some allowance for a distance dependence in this migration can be incorporated by adjusting the effective adjacent well distribution function given in Eq. (16). A reduction in hopping probability which is inverse linear or inverse quadratic in the separation distance X could be allowed for by altering the X^3 weighting in Eq. (16) to X^2 or X, respectively. For example, the inverse quadratic variation leads to the exponent in Eq. (17) being replaced by $-D_{\text{eff}}\Delta/\bar{l}^2(1-[1-(\pi q\bar{l})^2]/[1+(\pi q\bar{l})^2])$. Given the wide variation in well sizes inherent in the exponential distribution, such an allowance for well hopping variability is probably essential.

While the PW model, represented by Eq. (17), may allow for interpore migration effects in the echo attenuation, the pore equilibration approximation inherent in its derivation must break down for sufficiently large values of the well dimension, l. Furthermore, the derivation takes no account of relaxation effects which may occur at the barriers. By contrast, the IRW model [Eq. (14)], while accounting for relaxation effects and avoiding the pore equilibration assumption, takes no account of migration between pores. Both models are characterized, to first order, by the well distribution structure factor predicted by the simple infinite time diffraction relation of Eq. (8). It is in the q- and Δ-dependent deviations from this behavior that distinctions arise. Both models result in enhanced echo decay at higher q values, by comparison with that predicted by the well structure factor alone. However, a significant distinction arises when considering the Δ dependence of the signal. For IRW, a family of echo attenuations obtained at different observations times Δ will have a common q dependence at long times but deviate toward higher echo amplitudes for $\Delta \lesssim l^2/2D$. By contrast, for PW the increasing decay of echo amplitude proceeds relentlessly as Δ is increased, owing to the leakage from the wells which is characterized by the parameter D_{eff}.

IV. RESULTS

Echo attenuation data for the conduction electrons in Fluoranthene have been obtained at four different observation times, Δ for at least two different δ values. The shortest of these, 10 μs, was determined by the need to allow sufficient receiver recovery time after the 180° rf pulse, while the longest time, 19.5 μs, was determined by the need for sufficient signal-to-noise ratio in the face of relaxation decay of the echo amplitude ($T_2 \approx 7$ μs). In Fig. 2 some of these data, corresponding to the shortest duration gradient pulse (around 2 μs), are plotted on a conventional Stejskal-Tanner plot as $\ln(E(q,\Delta))$ vs

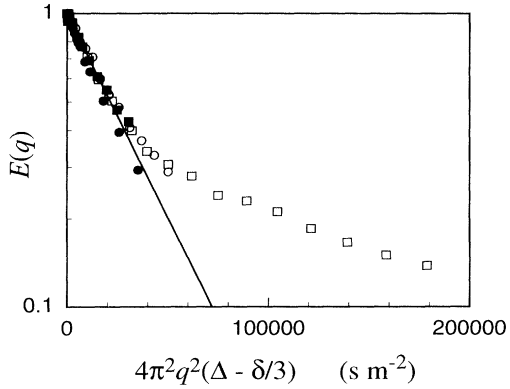

FIG. 2. Log of normalized echo amplitude vs $4\pi^2q^2\Delta_r$ (Stejskal-Tanner plot) for electron-spin echoes obtained from $(FA)_2PF_6$. The data shown are for a range of reduced diffusion times ($\Delta_r=\Delta-\delta/3$) and in each case correspond to the shortest gradient pulse duration, $\delta=2$ μs for $\Delta=10$ μs (filled circles), 14 μs (open circles), and 16.5 μs (filled squares), and to $\delta=2.6$ μs for $\Delta=19.5$ μs (open squares). The data deviate from the simple Gaussian expected for free diffusion with unique diffusion coefficient D, and do not lie precisely on a common curve as Δ is varied. This latter feature is characteristic of restricted diffusion.

$4\pi^2q^2\Delta_r$, where Δ_r is the effective gradient pulse separation, $\Delta-\delta/3$. (This reduction is the standard correction which is made to allow for diffusion during a square gradient pulse of duration δ. While it represents only an approximation to the result for half-sinusoidal pulses, the correction is slight and of no significance in the present context.)

It is clear that the data do not follow the Gaussian dependence expected for free diffusion, in which $\ln(E(q,\Delta))$ should vary linearly as $4\pi^2q^2\Delta_r$ with a slope given by the diffusion coefficient. Furthermore, the data cannot be explained by a distribution of diffusion coefficients owing to the lack of commonality of the set as the observation time Δ is increased. Indeed, the apparent reduction in slope with increasing Δ is exactly what one would expect if diffusive barriers were acting, thus reducing the apparent diffusion coefficient as the time of observation is increased. The data therefore present a *prima facie* case for proposing a model involving restricted diffusion.

An initial analysis of the low-q data using the approximate echo attenuation expression $\exp[-(2\pi q)^2\frac{1}{12}\overline{l^2}]$ yields a value for $(\overline{l^2})^{1/2}$ of 80 ± 5 μm. From the number distribution $p(l)$ it may be shown that $(\overline{l^2})^{1/2}=\sqrt{6}\,\overline{l}$ and, hence, $\overline{l}\approx33$ μm.

Next we have attempted to fit the data sets, for each observation time Δ, using the IRW model in which we assume the exponential distribution of well lengths expected on the basis of the random defects model. In fitting the data to Eqs. (12) and (13) we have used a least-squares algorithm in which $\overline{l}$ and M are the free parameters, with D being fixed at the value of 1.8×10^{-4} m^2 s^{-1} used in the previous steady gradient work,[2] noting that the fits to $\overline{l}$ depend only weakly on D. In the case of all the data sets we noticed that a small correction of around 10% was needed in the assigned gradient pulse widths for 2.6 and 2.0 μs in order to produce compatibility with the data obtained for $\delta=4.0$ μs. We attributed this effect to slight deviations from the half-sinusoidal shape for the shorter pulse widths and the consequent difficulty in assigning an effective q value. Only the low-q data were considered in making this adjustment, since here the echo attenuation must follow the $\exp[-(2\pi q)^2\overline{X^2}]$ relation, irrespective of any assumption regarding the restrictions to diffusion. While all our subsequent figures and fits incorporate this correction, we emphasize that the conclusions reached here are not significantly dependent on this adjustment.

Figure 3(a) shows an example of the data for the observation time Δ of 16.5 μs along with the best fit using Eqs. (12) and (13). We have carried out similar fits for each of the observation times Δ of 10, 14, 16.5, and 19.5 μs. A compromise simultaneous fit to all data is shown in Fig. 3(b). The parameters for all of the fits are summarized in Table I. Except for the shortest times of $\Delta=10$ and 14 μs, the data yield fairly consistent values of $\overline{l}$ around 50 μm, and M on the order of 0.1. The value of the wall sink density corresponds to the fast diffusion regime $Ml/2D\ll1$ for the overwhelming majority of the wells within the exponential distribution, and an additional well-size-dependent relaxation time of $l/2M$, corresponding to 250 μs at the mode well spacing $\overline{l}\approx50$ μm. The fitted transverse relaxation time, caused largely by spin-lattice interactions,[18] is $T_2\approx7$ μs. Consequently, and without attempting to speculate on the possible mechanism for M, the effect of wall relaxation is weak except for barrier spacing much shorter than 5 μm. However,

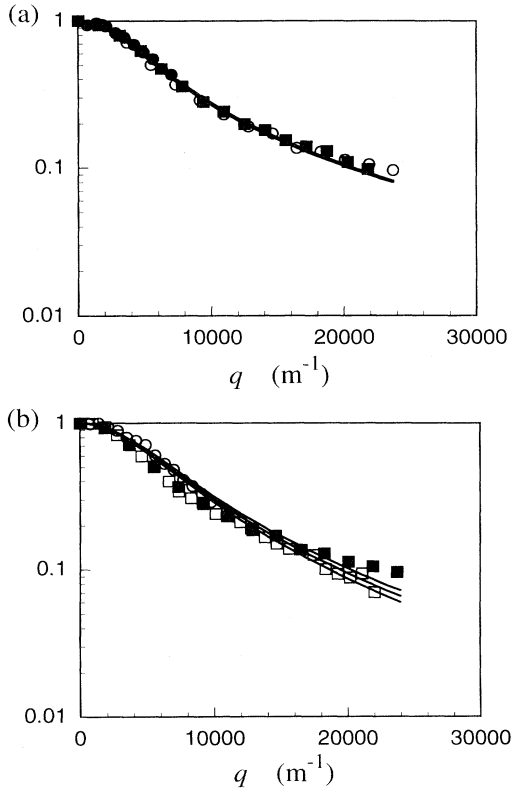

FIG. 3. Log of normalized echo amplitude vs q for electron-spin echoes from $(FA)_2PF_6$. (a) shows the case of the observation time $\Delta=16.5$ μs (closed circles are $\delta=2.0$ μs, open circles are $\delta=2.6$ μs, and closed squares are $\delta=4.0$ μs). Also shown is the best fit using the impenetrable relaxing wall (IRW) model optimized by varying M and $\overline{l}$. The parameters for the fits to all the data corresponding to the different observation times are summarized in Table I. (b) shows superposed data for (Δ,δ) values of open circles (14.0 and 2.0 μs), closed squares (16.5 and 2.6 μs), and open squares (19.5 and 2.6 μs) along with the set of three IRW curves corresponding to the compromise best-fit parameter set ($D=1.8\times10^{-4}$ m^{2}s^{-1}, $\overline{l}=47$ μm, and $M=0.01$), where the descending amplitude corresponds to ascending Δ.

TABLE I. Parameters used in fits to the data shown in Fig. 3 using the IRW model.

$\overline{l}$ (μm)	M (m s^{-1})	D (m^2 s^{-1})	Δ (μs)
21	4	1.8×10^{-4}	10.0
20	4	1.8×10^{-4}	14.0
47	0	1.8×10^{-4}	16.5
46	0.11	1.8×10^{-4}	19.5
47	0.01	1.8×10^{-4}	average best fit

these short wells will dominate the remaining echo amplitude at the largest values of q, so that the effect of this relaxation in the fitting of the echo attenuation data is important.

The discrepancy in fitting the IRW model to the data sets obtained at different observation times Δ naturally leads to our considering the alternative PW description. This latter model is lent further credence by the trend, apparent across the range of Δ values used in this work, to somewhat greater attenuation of the echo as Δ is increased. In consequence we have carried out a least-squares analysis of the echo attenuation data depicted in which the fit using Eq. (17) is optimized by varying D_{eff} and $\bar{l}$. For the uniform hopping PW model depicted in Eq. (17), no good fit is obtained in which $D_{\text{eff}} \neq 0$. By contrast, the inverse quadratic dependence of well hopping on well separation does yield a fairly consistent family of fitted curves. An example of one such fit ($\Delta = 16.5$ μs) is shown in Fig. 4(a), while the combined data fit is shown in Fig. 4(b). The parameters for all these fits are summarized in Table II. The slight superiority of this model over IRW is apparent in the combined data fit. By comparison with the IRW family shown in Fig. 3(b), the PW description is more compatible with the data obtained over a range of values of Δ. It is also clear that the value of $\bar{l}$ obtained in the PW fit is, at 27 μm, somewhat closer to the estimate of 33 μm obtained using the low-q data.

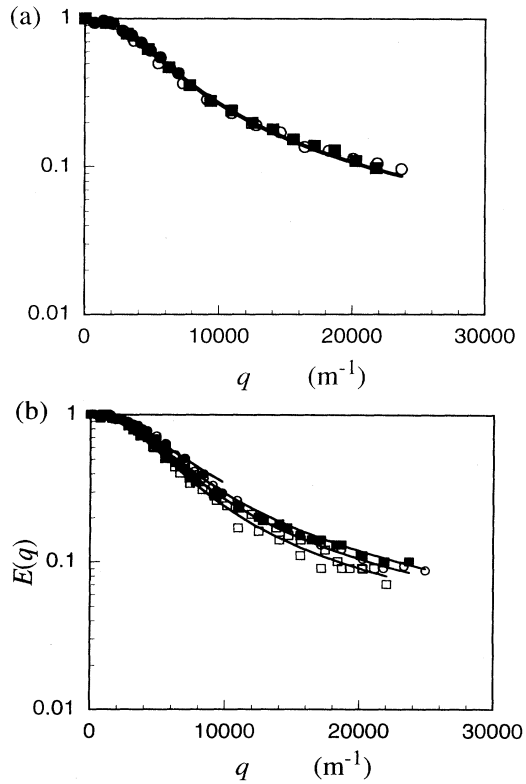

FIG. 4. As for Fig. 3, but with fits carried out using the permeable well (PW) model optimized by varying D_{eff} and $\bar{l}$. The fitted parameters are shown in Table II. No good fit is found assuming a uniform hopping rate, and the theoretical curves shown correspond to an assumption of inverse quadratic dependence of well hopping on well separation. The combined data fit is shown in (b), in which the data for $\Delta = 10$, 14, 16.5, and 19.5 μs are shown as closed circles, open circles, closed squares, and open squares, respectively. The four PW curves correspond to the best-fit parameters to the entire data set ($D_{\text{eff}} = 2.1 \times 10^{-5}$ m^2 s^{-1}, $\bar{l} = 25$ μm), where the descending amplitude corresponds to ascending Δ.

It might reasonably be argued that the analysis so far presented is dependent upon an assumed exponential distribution of well sizes. In principle, given a knowledge of the specific nature of the electron-barrier interaction, the echo attenuation function could be appropriately transformed to yield the appropriate weight distribution function $p(l)$. While we have not attempted to carry out an inverse transformation of the echo attenuation data using Eq. (12) and (16), we have been able to approximate this by utilizing the first-order time-independent diffraction model. Because of the Fourier relation inherent in Eq. (6), we may carry out this analysis by performing an inverse Fourier transformation (FT) and then fitting the data to a sum of one-dimensional well autocorrelation functions. Because of the inherent assumption of the long-time limit for all wells, we have only attempted this for the longest observation time data for which $\Delta = 19.5$ μs. The FT of this data is shown in Fig. 5 along with the corresponding distribution function $p_{\text{eff}}(l)$. Also shown are the exponential weight function $p(l)$, using the value $\bar{l} = 25$ μm. It should be noted that the method of analysis involves the least-distance (LDP) algorithm due to Lawson and Hanson,[19] in which the kernel is taken to be the expected triangular autocorrelation function. It can be seen that the resulting weight function is truncated for values of l below 5 μm. Such a cutoff was earlier proposed in the analysis of steady gradient data.

It should be noted that the inversion process is not at all unique. For example, a different algorithm [for example, non-negative least squares (Ref. 19)] yields a different distribution function. Furthermore, the direct inversion process assumes perfectly trapped electrons, no relaxation, and a long diffusion time limit, whereas the fits to the echo attenuation data using the exponential distribution takes account of relaxation, wall permeability, and finite diffusion time effects. Consequently, we place more weight on the exponential distribution fits used here. We include the inversion calculations in order to demonstrate the analysis potential of the PGSE method under condi-

TABLE II. Parameters used in fits to the data shown in Fig. 4 using the PW model.

$\bar{l}$ (μm)	D_{eff} (m^2 s^{-1})	Δ (μs)
13	3.2×10^{-5}	10.0
20	2.2×10^{-5}	14.0
26	2.1×10^{-5}	16.5
26	2.1×10^{-5}	19.5
25	2.1×10^{-5}	combined fit

tions where the shape of the displacement propagator, $\overline{P_s}$, is well known.

Finally we have attempted to fit the data presented here with a model comprising two populations of electrons, one of weight x which is free to diffuse without restriction with self-diffusion coefficient D, and one of weight $1-x$ which is completely confined. The best fit to D and x is shown in Fig. 6, and clearly gives a poor representation of the data.

V. DISCUSSION AND CONCLUSIONS

So far we have not considered the problem of transverse migration of electrons.[1] While diffusional motion transverse to the conducting channels cannot in itself lead to echo attenuation if the single crystal is properly aligned, the facility to hop between channels over the PGSE observation time may lead to an entirely different motional averaging process. In particular, if electrons are able to sample many different well sizes over the time Δ, the net migration in the axial direction parallel to those channels will be quite different than if the electrons were confined to a single local well dimension with the echo signal being averaged over the well size distribution.

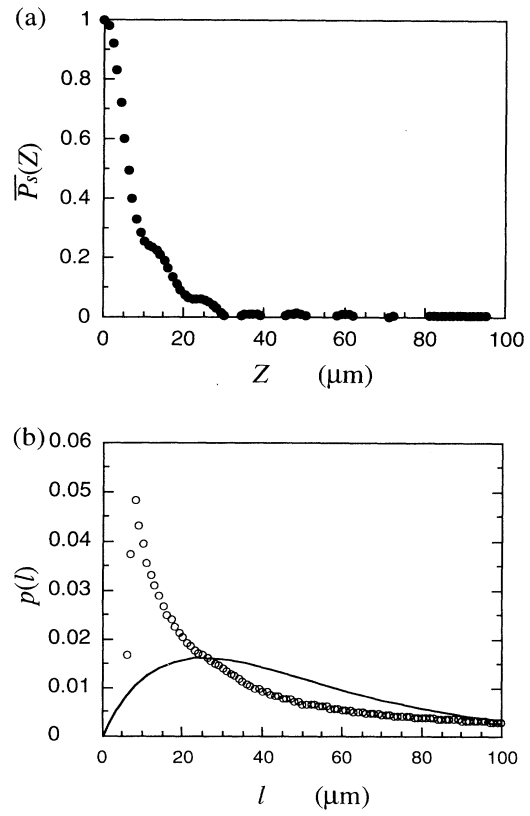

FIG. 5. (a) The spatial Fourier transform of the $E(q)$ data for $\Delta=19.5$ μs and $\delta=2.6$ μs along with (b) the corresponding distribution function $p_{\text{eff}}(l)$ obtained using the LDP (open circles) algorithm of Lawson and Hanson in which the kernel is taken to be the expected triangular autocorrelation function. The solid curve shows the exponential weight function $p(l)$, calculated using the value $\bar{l}=25$ μm.

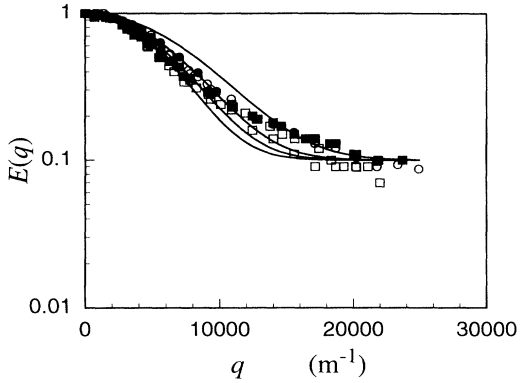

FIG. 6. Fit to the $E(q)$ data of Fig. 4(e) ($\Delta=10$, 14, 16.5, and 19.5 μs as closed circles, open circles, closed squares, and open squares, respectively) using a simple two-site model in which one fraction of electrons is able to diffuse freely ($D=3\times10^{-5}$ m^2s^{-1}, $x=0.9$), while the remaining electrons are confined. Descending amplitude corresponds to ascending Δ. The data are poorly represented by such a model.

In order to take account of this possibility, we have carried out some Monte Carlo simulations of this motion using a model in which electrons are allowed to hop between wells of differing size on a time scale τ which may be less than or greater to the time l^2/D taken to collide with the walls of the local well. In such a model not only the wall spacing is allowed to change between jumps but also the wall positions. In consequence the electrons find themselves hopping in a maze which, in principle, allows long-range motions. Our simulation results unambiguously demonstrate that the diffusional motion will be practically free, with a diffusion coefficient approaching the unrestricted value D when $\tau \ll l^2/D$. This observation is consistent with our intuitive understanding. The overall propagator is simply the convolution of N successive propagators corresponding to successive chain residencies of duration τ where $\Delta=N\tau$. Consequently, if $\tau \ll l^2/D$, then these propagators will be locally Gaussian and the net propagator will be a Gaussian of rms width $2D\Delta$. Such behavior would be expected given the upper estimate of transverse electron diffusion of around 1×10^{-6} m^2s^{-1}, since this would correspond to $\tau\sim10^{-8}$ s, for which the distance diffused along the conducting channel is on the order of 1 μm.

One of the most compelling features of our data is the flattening of the echo attenuation at large wave vector, which can only arise from electrons trapped in regions of small ($<$ 10 μm) dimension. Hopping which results in jumps between wells with shifting walls will release these trapped electrons, and the high-q data will be strongly attenuated. In consequence any lateral mobility must not be associated with hops between wells of differing and uncorrelated wall positions. Indeed we would suggest that the data presented here are only consistent with the conducting channels subtending many chains, so that, despite interchain hopping, electrons are confined to a single effective well over the 10–20-μs observation time associated with our method.

A schematic visualization of a possible well distribu-

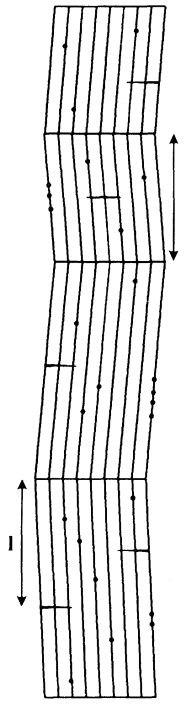

FIG. 7. Schematic representation of possible well distribution geometry. The grain tilting is highly exaggerated in comparison with the known value of diffusion perpendicular to the conducting channels. The dots represent scattering centers which limit conductivity while diffusion is hindered by at the horizontal lines, believed to correspond to grain boundaries and defects.

tion geometry leading to our observations is depicted in Fig. 7. As stated above, the reported upper limit on $D_\perp$ (Ref. 1) may be used to calculate the transverse motion of up to 1 μm during Δ. Thus it is clear from the figure that while electrons can easily sidestep the many barriers (shown as dots) encountered along individual fluoranthene channels, the much larger barriers, over 1 μm across and typically $\bar{l}$ apart, will confine many of the spins to single wells of small ($<\bar{l}$) dimensions, with the associated flattening of the attenuation curves. A well situation, as depicted in Fig. 7, could be formed by grain boundaries of a mosaiclike crystal structure that may exist in the system.

The IRW and PW analyses of the echo attenuation data presented above do not of course represent unique solutions to the problem of the conduction-electron diffusion and the motional barriers appropriate to fluoranthene. However, it may be concluded that the one-dimensional well model based on an appropriate distribution of well sizes does give a reasonable representation, and over a range of diffusion observation time covering a factor of 2. In particular, we note a much weaker dependence of the echo attenuation upon observation time Δ than would be expected for unrestricted diffusion. Furthermore, the overall q dependence of the data broadly follows the first-order diffraction prediction based on an exponential distribution of one-dimensional wells. The fits using both the IRW and PW variants on the diffraction model yield mean well size values broadly consistent with an estimate based on the low-q data. Further credence is lent to the first-order diffraction interpretation by some of the finer details within the data. For example, in both $\Delta=16.5$ and 19.5 μs, where the echo attenuation was measured to high-q values, one may discern differences which are consistent with the anomalies expected due to diffusion during the finite width gradient pulse. The flattening of the curves at high q arises from the presence of electrons in the smaller wells for which the echo attenuation is considerably less. In both cases of observation time the $\delta=4.0$-μs data at large wave vector lie above that at $\delta=2.6$ μs, consistent with the expected reduction in apparent well size.

It is clear that the estimates on the well dimension parameter $\bar{l}$ obtained in this work differ markedly from that calculated on the basis of the steady gradient analysis.[2] We attribute this to the approximations inherent in that analysis, and in particular the Gaussian phase assumption which, while reliable to first order, cannot represent the echo attenuation effectively under conditions of high attenuation.[4] It is precisely the region of very large signal attenuation which must be used to fit the steady gradient spin-echo data for $p(l)$. As pointed out in Sec. I, the PGSE ESR experiment simultaneously explores the two parameter domains of the scattering wave vector q and diffusion time Δ. It should therefore provide a more reliable basis of analysis in which the spin-phase variations which arise from diffusional displacements can be clearly separated from those which arise from transverse relaxation.

Finally, it may be noted that $(FA)_2PF_6$ is not the only system amenable to PGSE ESR investigation. Obvious candidates include members of the organic conductors family, such as other fluoranthenes, as well as conducting pyrene, perylene, and napthalene compounds. Most of these materials exhibit sufficiently narrow ESR lines[20] and substantial electronic diffusion to be considered suitable for further studies related to electronic motion.

ACKNOWLEDGMENTS

We are grateful to J. Gmeiner for preparing the single crystals used in this study. Financial support by the New Zealand Foundation for Research, Science and Technology is acknowledged by P.T.C., and from the DFG (SFB 195) by R.R. and E.D.

[1]G. G. Maresch, A. Grupp, M. Mehring, J. U. v. Schütz, and H. C. Wolf, J. Phys. (Paris) **46**, 461 (1985).
[2]R. Ruf, N. Kaplan, and E. Dormann, Phys. Rev. Lett. **75**, 6 (1995).
[3]H. C. Torrey, Phys. Rev. **104**, 563 (1956).
[4]C. H. Neumann, J. Chem. Phys. **60**, 4508 (1974).
[5]E. O. Stejskal and J. E. Tanner, J. Chem. Phys. **42**, 288 (1965).
[6]P. T. Callaghan, *Principles of Nuclear Magnetic Resonance Microscopy* (Oxford Unversity Press, Oxford, 1991).
[7]P. T. Callaghan, A. Coy, T. J. P. Halpin, D. MacGowan, K. J. Packer, and F. O. Zelaya, J. Chem. Phys. **97**, 651 (1992).
[8]A. Coy and P. T. Callaghan, J. Chem. Phys. **101**, 4599 (1994).
[9]P. T. Callaghan, A. Coy, R. Ruf, E. Dormann, and N. Kaplan, J. Magn. Res. A **111**, 127 (1994).
[10]C. J. Rofe, J. Van Noort, P. J. Back, and P. T. Callaghan, J. Magn. Res. B **108**, 125 (1995).
[11]M. Conradi, A. N. Garroway, D. G. Cory, and J. Miller, J. Magn. Res. **94**, 370 (1991).
[12]S. Sachs and E. Dormann, Synth. Met. **25**, 157 (1988).
[13]J. Kärger and W. Heink, J. Magn. Res. **51**, 1 (1983).
[14]P. P. Mitra and B. I. Halperin, J. Magn. Reson. A **113**, 94 (1995).
[15]J. E. Tanner and E. O. Stejskal, J. Chem. Phys. **49**, 1768 (1968).
[16]See P. T. Callaghan and A. Coy, Phys. Rev. Lett. **68**, 3176 (1992); *Principles of Nuclear Magnetic Resonance Microscopy* (Ref. 6), p. 372.
[17]P. T. Callaghan, J. Magn. Res. A **113**, 53 (1995).
[18]G. Sachs, Ph.D. dissertation, University of Bayreuth, 1987, p. 113.
[19]C. L. Lawson and R. J. Hansen, *Solving Least Squares Problems* (Prentice-Hall, New York, 1974).
[20]E. Dormann, Phys. Rev. B **39**, 221 (1983).